IEEE Access
Multidisciplinary | Rapid Review | Open Access Journal

IEEE PHOTONICS SOCIETY SECTION

Received 23 December 2023, accepted 30 January 2024, date of publication 6 February 2024, date of current version 19 March 2024.

Digital Object Identifier 10.1109/ACCESS.2024.3363453

RESEARCH ARTICLE

Optical Upconversion of OFDM Signals for Next Generation Fronthauling Using Frequency Doubling and Quadrupling

S. J. SREERAJ[1], (Graduate Student Member, IEEE), B. LAKSHMAN[1], (Graduate Student Member, IEEE), RADHAKRISHNA GANTI[1], (Member, IEEE), AMPALAVANAPILLAI NIRMALATHAS[2], (Senior Member, IEEE), R. DAVID KOILPILLAI[1], (Member, IEEE), AND DEEPA VENKITESH[1], (Member, IEEE)

[1]Department of Electrical Engineering, Indian Institute of Technology Madras, Chennai, Tamil Nadu 600036, India
[2]Department of Electrical and Electronic Engineering, The University of Melbourne, Melbourne, VIC 3010, Australia

Corresponding author: Deepa Venkitesh (deepa@ee.iitm.ac.in)

The project was funded by (i) Department of Telecommunication (DoT), Govt. of India, for the indigenous 5G Testbed Development Project, (ii) Department of Science and Technology (DST), India and Ministry of Human Resource Development (MHRD), India under the IMPRINT-IIC scheme for supporting this work, and (iii) Team Research Project Grant of Indian Institute of Technology, Madras, and in part by (iv) Scheme for Promotion of Academic and Research Collaboration (SPARC), Ministry of Education, India.

ABSTRACT Fronthaul data rates in case of millimeter wave (mmWave) wireless systems scale up to several Gbps in the currently deployed digitized radio over fiber solutions, resulting in large complexity remote radio heads (RRHs). We propose a promising solution involving optical frequency doubling and quadrupling, where all complex digital processing are moved to the centralized base band unit (BBU), thereby allowing placement of large number of low-complex RRHs at long distances. We experimentally demonstrate optical frequency doubling and quadrupling for the generation and transport of millimeter wave mmWave signals with OFDM containing QPSK, 16/64/256-QAM modulation formats over a distance of 2 km. These schemes enable the use of low-frequency RF signals at the BBU for the generation of mmWaves at the RRH. We evaluate the performance of the systems in terms of error vector magnitude (EVM) and out-of-band emissions of the upconverted data. Our results show that the proposed schemes achieve EVM values within the 3GPP 5G standard requirements. We also investigate the tunability and scalability of the proposed schemes across the n258 band (24.25 - 27.5 GHz) and discuss the feasibility of implementing dense wavelength division multiplexing (DWDM) for servicing multi-channel operation required for multisector antennas. The proposed schemes can support high data rate transmission for future wireless networks including 6G.

INDEX TERMS Analog radio over fiber, fronthaul, frequency doubling, frequency quadrupling, optical upconversion, mmWave 5g, mmWave generation, EVM.

I. INTRODUCTION

The demand for data is growing rapidly as more devices connect to the internet and consume more digital content and services. 5G, the latest generation of mobile network technology, promises to provide higher data rates, lower latency and more capacity than the previous generations [1], [2]. While the sub 6 GHz implementations of 5G are already commonplace and the mmWave implementations are mostly limited to urban deployments; the next generation 6G is also envisaged [3], [4], [5], [6]. High bandwidth and low latency applications in different sectors,

The associate editor coordinating the review of this manuscript and approving it for publication was David Caplan.

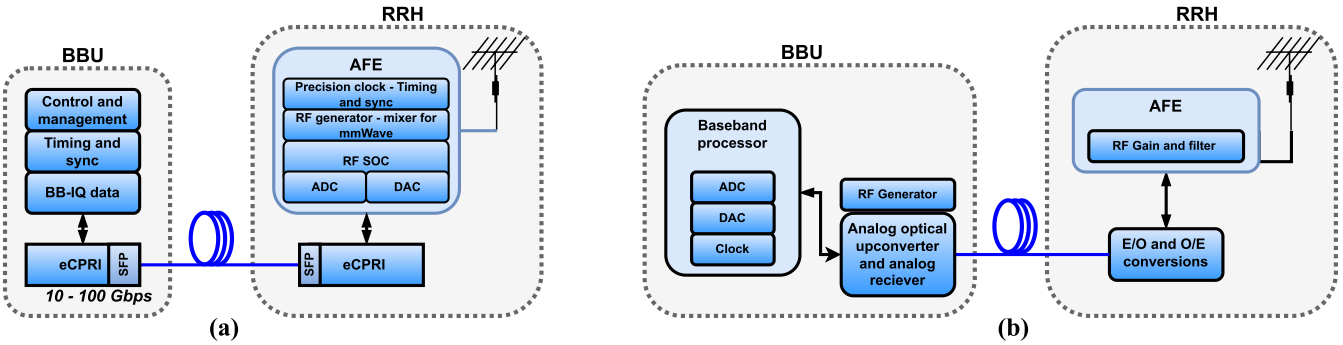

FIGURE 1. (a) Conceptual diagram of CRAN architecture with eCPRI fronthaul below split-8, and (b) ARoF fronthauling. CRAN - centralized radio access network, eCPRI - enhanced common public radio interface, RFSOC - radio frequency system on chip, AFE - analog front end, E/O - electrical to optical, O/E - optical to electrical, ARoF - analog radio over fiber.

such as entertainment, gaming, augmented reality, virtual reality, health care, education, manufacturing, transportation, human-machine interfaces, and blockchain, require that high-frequency spectra are allotted for these services [7], [8], [9]. They offer several benefits over the lower frequency bands, such as larger bandwidth, higher spatial resolution, smaller antenna size, and relatively less interference and flexibility of frequency reuse [10], [11]. The cell architecture is expected to transition from small cells to nano cells because of challenges such as higher propagation loss, atmospheric absorption, rain fading and blockage by obstacles. Therefore, future networks need to employ advanced techniques such as massive Multiple-Input and Multiple-Output (MIMO), beamforming, beam tracking, and network densification to overcome these challenges to exploit the potential of millimeter waves.

The conventional radio access network (RAN) uses digitized radio over fiber (DRoF) to transport data from baseband units (BBUs) to remote radio heads (RRHs). The current DRoF standard is enhanced common public radio interface (eCPRI), which supports ethernet rates from 10 Gbps to 100 Gbps. The actual user data transmitted via CPRI also depends on the CPRI split used. For example, for a 100 MHz bandwidth with 256-QAM, 8 MIMO layers and 32 antenna ports, a CPRI split-3 requires a downlink line rate of 4 Gbps, while the same user data for CPRI Split-7 requires up to 22 Gbps [12]. However, the lower split approach requires increased complexiety at the RRHs, such as analog to digital converters (ADC), digital to analog converters (DAC), upconverters, RF sources, and synchronization systems. Fig.1(a) shows the schematic of eCPRI fronthaul architecture in a lower split (below split 8), where the baseband data is digitized and transported through fiber to the RRH. In the RRH, the DAC in RF system on chip (RFSOC) converts it into an analog baseband signal, before being upconverted to the target frequency. Similarly, in the uplink path, an ADC digitizes the incoming signal to be transported to the BBU. A 4-sector antenna operating with 100 MHz bandwidth described earlier requires a fronthaul datarate of 80 Gbps with split-7. Further complicated are the timing synchronization requirements between BBU and RRH, for which even GPS clocks are used [13], and even stricter synchronization requirements exist for advanced transmission technologies such as coordinated multipoint (CoMP) [14].

Analog radio over fiber (ARoF) systems provide a promising solution for avoiding RAN fronthaul complexity by moving all complex processing to the centralized BBU and thus allowing low-cost RRHs placed at long distances. ARoF systems can significantly reduce latency (depending on BBU-RRH distance), facilitate advanced wireless cooperation technologies, and offer a cost-effective solution with future-proof deployment [15]. The use of radio frequency over fiber (RFoF) technologies with direct/external modulation techniques operating at high frequencies offers a simple solution, but they suffer from dispersion-induced fading. Although single-sideband (SSB) modulation overcomes the dispersion-induced effects, the system requires high-frequency RF sources and electro-optic modulators. Optical upconversion schemes provide the advantage of generating mmWave remotely at the RRH with low-frequency RF sources. Chasing the options of analog optical fronthaul for next-generation wireless systems, experimental feasibility studies are conducted exploring in academia and industry [16], [17], [18]. Integrated solutions for basic ARoF transceivers, upconverters, downconverter and with multiplexing/multiple-access options such as space division multiplexing (SDM), wavelength division multiplexing (WDM) and reconfigurable optical add/drop multiplexers (ROADM) are investigated for scaling the infrastructure [19], [20], [21].

Compared to the methods for optical generation of RF signals such as optoelectronic oscillators [22], [23], optical injection locking [24], and optical phase locked loops [25], external modulator based upconversion approaches offer a relatively simple, flexible and integrable solution [26], [27]. While optical doubling schemes such as [18] require optical filters to avoid unwanted harmonic components, schemes that employ cascaded Mach-Zehnder modulators (MZM) for

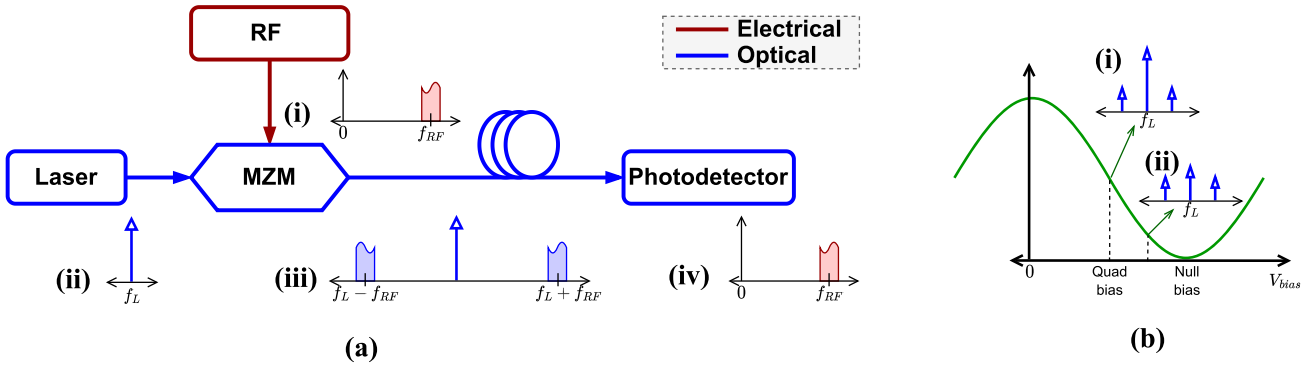

FIGURE 2. (a) Block diagram of a simple analog radio frequency-over-fiber (RFoF) link with external modulation scheme. Inset figures show the spectra of (i) RF passband signal (ii) laser source, (iii) laser modulated with RF passband signal, (iv) electrical output after photodetection. (b) Transfer curve of MZM and the expected spectra at different bias points such as quad and low bias - shown in (i) and (ii) respectively.

tone and upconversion [20] do not require filters. While filter-less optical mmWave generations with quadrupling were demonstrated in early studies [28], [29], [30], [31], no demonstration was reported for practical implementations with 3GPP specified 5G signals upto 256-QAM - to the best of the knowledge of the authors.

We had demonstrated transport of data through optical doubling and quadrupling earlier [32], [33]. In this work we demonstrate schemes to transport a 100 MHz OFDM signals with up to 256 QAM modulation constellations over 2 km fiber with within 3GPP specified EVM levels. Both schemes are optimized for best EVM performance based on bias point and input RF power. We also comment on the energy requirements in RRH for both DRFoF and proposed scheme. The remainder of the paper is organized as follows. Section II discusses various analog optical fronthauling schemes along with critical signal quality requirements, which, in turn, decide the performance metrics. Section III discusses the experimental setup of analog optical doubler and quadrupler, transporting 100 MHz OFDM signal at the *n258* band. Detailed performance analysis with various modulation formats, RF frequencies and multiband operation is discussed in Section IV, and the results are summarised in Section V.

II. ANALOG OPTICAL SCHEMES FOR FRONTHAULING

Analog optical fronthaul methods are mainly categorized into three - (i) *baseband over fiber* (BBoF), (ii) *intermediate frequency over fiber* (IFoF), and (iii) *radio frequency over fiber* (RFoF). As the name indicates, BBoF transports baseband signals directly over optical fibers without any frequency conversion and has the advantage of simplicity and low cost, but it requires a high-frequency upconversion stage at the RRH to generate the modulated RF signals for transmission. The IFoF method converts baseband signals to intermediate frequency (IF) signals before modulating them onto optical carriers. It has the advantage of higher bandwidth compared to BBoF, but it still requires a frequency upconversion stage at the RRH to generate the RF signals for wireless transmission. RFoF methods deliver high-frequency radio signals to the RRH either by direct/external modulation formats or by employing optical upconversion.

Fig. 2.(a) shows an RFoF system realized with an MZM, along with spectra at each stage. An MZM follows a cosine squared transfer function, and for linear operation, the standard operating point of an MZM is the quadrature point, which provides a double sideband (DSB) with carrier signal (Fig.2.(b).(i)). Operating the bias point more towards the null point of the modulator is usually termed as 'low biasing', which provides a DSB signal with carrier power relatively lower compared to quadrature bias.

RFoF has the advantage of supporting multiple wireless standards and bands with a single fiber link, and it does not require any upconversion stage at the RRU. However, it requires high-frequency electrical-to-optical (E/O) converters and high-frequency RF generators. RFoF-based optical upconversion methods offer the advantage of using low-frequency E/O converters at the modulator stages. In this work, we demonstrate optical upconversions schemes - doubling and quadrupling for mmWave 5G fronthauling. Optical doubler and quadrupler, with double sideband (DSB) and single sideband (SSB) modulation formats, are discussed, where we see that upconversion-based schemes are resilient to fiber dispersion as well.

A. ANALOG OPTICAL DOUBLER AND QUADRUPLER

Fig.3 shows the schematic for optical upconversion in both doubling and quadrupling schemes. The baseband data is IF modulated in the electrical domain (shown as Fig.3.(i)), which is in turn modulated on a laser (frequency f_L) using an MZM, as indicated as IF MZM in the figure. Note that this is a dual drive MZM (DDMZM) that could be operated in the double DSB or SSB configuration with 90^0 RF hybrid. The output of the IF MZM is fed to a MZM (referred in the figure as doubler MZM) in the doubler configuration [18], [34]. In case of quadrupler, the IF MZM output is fed to a dual parallel MZM (DPMZM), which is termed in the figure as quadrupler DPMZM [35], [36].

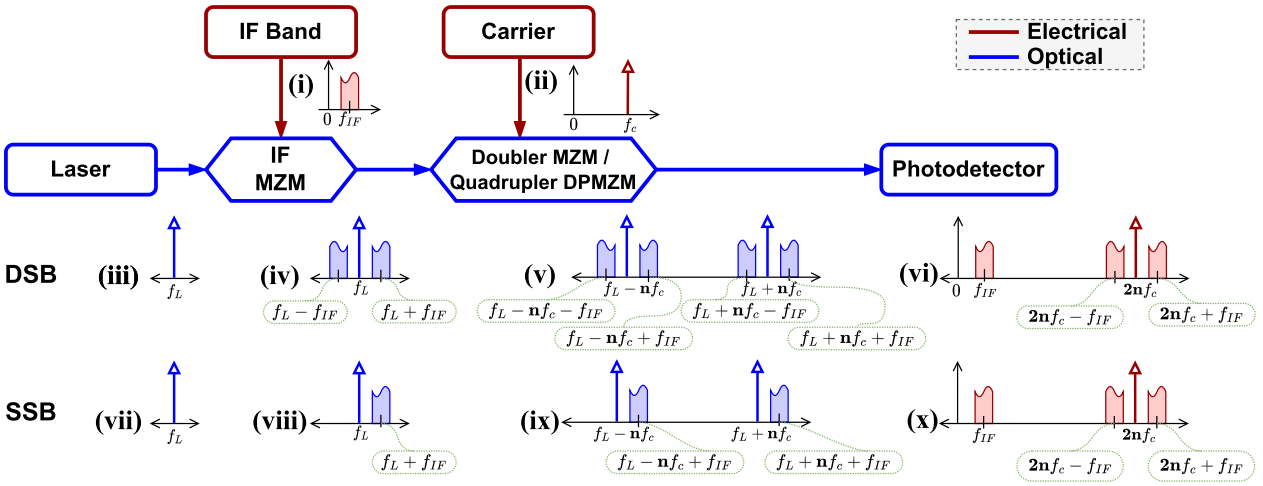

FIGURE 3. Conceptual block diagram of optical upconversion schemes and stage-wise spectra at each stage. For a doubler, and MZM is used in the second stage, and a DPMZM is used for the case of a quadrupler. In the spectra, for the case of doubler $n = 1$ and for quadrupler $n = 2$. The spectra for the cases of DSB and SSB modulations are shown parallelly.

The detailed analytical model for the optical doubler is given in [18], here we restrict to the conceptual description. The evolution of the spectra at the output of the laser, IFMZM, doubler MZM and photodiode are shown in Fig.3 (iii - vi), while the same for DSB case is shown in Fig.3 (vii - x). Note that the multiplying factor is $\mathbf{n} = 1$ for doubler and $\mathbf{n} = 2$ for quadrupler. The IF upconverted baseband is shown in 3 (i) and the RF carrier frequency to the multiplier modulators is shown in 3 (ii). If the desired output signal is at f_{RF}, and if the IF is at frequency f_{IF}, the required carrier frequencies to the multiplier stages are $(f_{RF} - f_{IF})/2$ and $(f_{RF} - f_{IF})/4$ for doubler and quadrupler configurations respectively. The desired output RF signal to be radiated will be generated at $2\mathbf{n}f_c + f_{IF}$, the details of which are discussed below.

In the doubler configuration, the doubler MZM is biased for a null point, which results in carrier suppression. A carrier suppressed double sideband signal (Fig.3.(v)) with its upper and lower sidebands centered at $f_L + f_c$ and $f_L - f_c$ respectively, along with the IF bands. The copies of the IF signal appear at $f_L - f_c \pm f_{IF}$, and $f_L + f_c \pm f_{IF}$. The optical signal, after falling on the photodetector, generates beat frequencies as a tone at $2f_c$ and data band copies at f_{IF}, the lower sideband (LSB) at $2f_c - f_{IF}$ and upper sideband (USB) at $2f_c + f_{IF}$, as shown in (Fig.3.(vi)). In this work, we chose the data band at the upper band ($2f_c + f_{IF}$), and uses RF filters to remove the other bands. Although a spectrally flipped replica of the data is available at the lower sideband with $f_{RF} = 2f_c - f_{IF}$, the carrier frequency to be used at the input of the multiplier/upconverter stage to achieve the desired modulated RF frequency is higher. For instance, if the desired frequency is 26 GHz and $f_{IF} = 2$ GHz, the f_c to be applied to the doubler MZM must be 14 GHz if LSB is used while it is only 12 GHz if the USB is used.

Note that, even though IF modulation can be carried out at relatively lower bandwidths, external modulation is preferred over direct modulation inorder to improve link gain, spurious free dynamic range (SFDR) and chirp resistance. External modulation also lends itself to control the unwanted carrier power through bias control [32].

In the case of quadrupler child modulators of the DPMZM are biased at the full point, and the parent modulator is biased at null point, and the RF ports are fed with 90^o phase shifted versions - which results in the carrier and first-order suppression [35], [36]. The spectral components follow a similar pattern as that of the optical doubler discussed above. The IF stages remain the same, while the spectral components shown in Fig.3.(v), and Fig.3.(vi) are to be set with $\mathbf{n} = 2$. It can be inferred that the carrier frequency required at the upconverter stage (f_c) is lower than that of the doubler. The spectra are shown in 3.(vii - x) correspond to the cases where the IF modulation is carried out in a SSB configuration. The simplest way to generate an SSB signal is to use a DDMZM, whose two input ports are fed with IF phase shifted by 90^o [18], [37]. Although the RF spectrum at the photodetector output appears the same in both DSB and SSB, the data band power in the case of SSB is reduced compared to a DSB format at short fiber lengths.

B. DISPERSION TOLERANCE

While the obvious advantage of an optical upconversion scheme is the requirement of low-frequency electro-optic components, they also have excellent dispersion tolerance for long distances compared to direct/external modulated RoF links. Fig. 4 shows a simulation of RF fading characteristics of various modulation formats discussed above, across the frequency (main figure) and length (inset figure). The figure shows the variation of a targeted passband frequency with an IF of 2 GHz and length of 5 km, and the inset figure shows the sample targeted data band of 26 GHz at various lengths. RF over fiber fading / dispersive fading is a well studied phenomenon and many methods are devised to overcome this effect [38], [39]. We can infer from these results that,

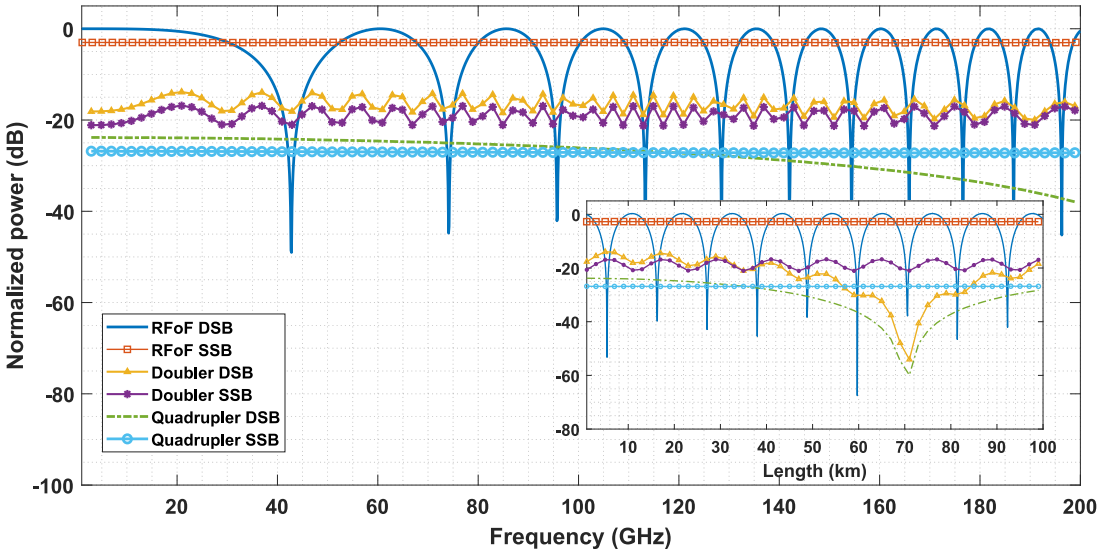

FIGURE 4. Simulation results of RF over fiber fading characteristics across frequency for various modulation formats. The inset figure shows the variation across length for a 26.4 GHz modulation.

moving to sub THz bands, which are potential candidates to 6G (116 GHz to 240 THz [40]), SSB modulation holds advantage, while for the mmWave ranges used in 5G, DSB and SSB are mostly same with respect to fading performance. In the lower frequencies and shorter lengths though, DSB holds the advantage of delivering higher power to the succeeding stages. It is observed from the simulation results in Fig. 4 (inset), the first null of a standard external modulation-based DSB signal is at 5.4 km, and that of the SSB version is ideally a flat response. Further, DSB versions employing specific upconversion formats (such as one used in this work), itself is more resilient to fading than a conventional DSB system, the phenomenon which is briefly studied in [29]. Fig. 4 indicates that the DSB versions of doubler and quadrupler degrade much slower with fiber length with its first null at 70.3 km, which is far better than the 5.3 km of standard DSB with RFoF. The upconverted SSB formats also follow nearly a flat response as that of standard SSB, and fully dispersion free, but have a power penalty of 3 dB compared to the DSB counterpart. Aperiodic fading characteristic is observed in the optical upconverted formats, which is a result of the interference from higher harmonics, also reported in [41].

C. TRANSMISSION SIGNAL QUALITY REQUIREMENTS

For the scope of this experiment, we refer to the specifications mentioned in 3GPP Release 16 for evaluating the critical signal quality requirements [42]. The candidate modulation formats for 5G NR are QPSK, 16 QAM, 64 QAM, and 256 QAM and the corresponding error vector measurement (EVM) requirements are given in Table.1 for each of the formats. For a Base Station Type 2-O, the EVM needs to be calculated at a specific distance over the air (OTA).

TABLE 1. EVM requirements for various modulation formats as specified by 3GPP.

	QPSK	16 QAM	64 QAM	256 QAM
EVM (%)	17.5	12.5	8	3.5

The minimum allowed power in the spurious tones appearing at harmonic of RF components in doubler and quadrupler configurations must be within the limits specified by operating band unwanted emissions (OBUE). The OBUE for the n258 band is limited at -5 dBm, while for protection of earth exploration satellite services (EESS), it should be < -9 dBm. The base station radiated transmission spurious emission limits in FR2 outside of the operating band are specified as < -10 dBm in the near bands of n258 and up to < -15 dBm in the next set of bands. While the limits are mentioned even to further ranges, the strongest tone in our experiment is expected in these bands ($2f_c$ for doubler and $4f_c$ for quadrupler). Note that the harmonic RF components can fall in either the operating band or the outside - depending on the chosen IF and RF frequencies. Given the highest OTA power limit is <33 dBm for a *Local Area Base Station (BS)* category, a harmonic suppression of > 48 dB is targeted in our experiments.

III. EXPERIMENTAL SETUP

Fig.5 shows the schematic of the experimental setup for optical doubler setup at 26.4 GHz. The arbitrary waveform generator (Keysight M8190A-14B) generates the baseband I and Q data at a sample rate of 491.52 Msps. Standard 5G NR physical downlink shared channel (PDSCH) frames with OFDM signal of 100 MHz bandwidth containing QPSK, 16-QAM, 64-QAM and 256-QAM are transmitted along with the demodulation reference signals (DMRS) frames.

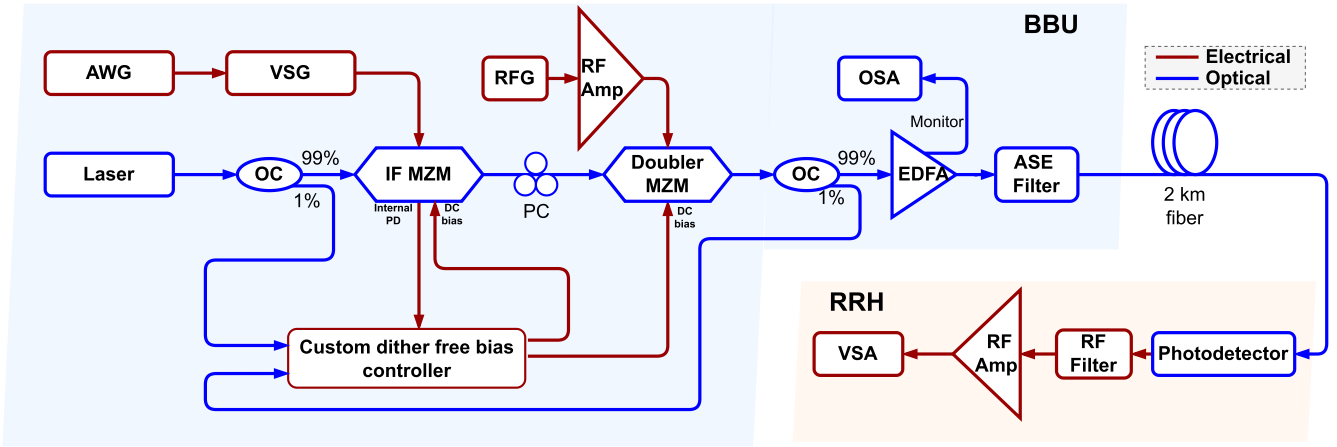

FIGURE 5. Experimental setup for data upconversion with optical doubler. AWG - Arbitrary waveform generator; VSG - Vector signal generator; RFG - RF Generator; OC - optical coupler; MZM - Mach Zehnder modulator; EDFA - Erbium-doped fiber amplifier; OSA - optical spectrum analyzer; PC - polarization controller; VSA - Vector signal analyzer.

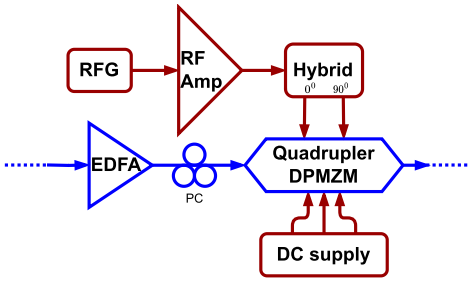

FIGURE 6. Implementation of frequency quadrupler in the same setup shown in Fig.5. The doubler MZM in Figure.5 is replaced with this setup. RFG - RF generator, EDFA - erbium-doped fiber amplifier.

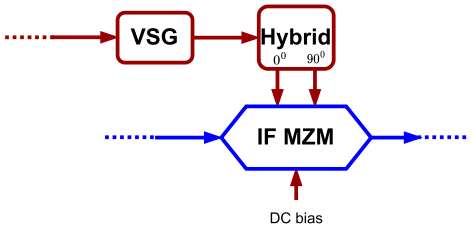

FIGURE 7. Setup for optical single sideband modulation. VSG - vector signal generator.

Subcarrier spacing of 30 kHz for 3276 filled subcarriers out of 4096 (FFT points) is chosen for transmission - which corresponds to 98.28 MHz occupied bandwidth. The vector signal generator (Keysight PSG E8257D) upconverts the I-Q data to the required IF. In this experiment, an IF of 3.2 GHz is chosen. The laser is tuned to emit at 1553.32 nm (ITU channel no 30) at 14.5 dBm, which is then fed to the IF MZM (Fujitsu FTM7937EZ) via a polarization-maintaining optical coupler (99/1). The optical power tap from the coupler and the internal photodiode of the MZM is used for bias control at a desired arbitrary bias point. The RF power at the input to the IF MZM and its bias points are varied to find the optimal region of operation of the ARoF link.

The IF-modulated signal is then fed to the optical doubler stage where the MZM is biased at null. The doubler MZM is fed with an RF tone of 11.6 GHz at a high modulation depth to aid the second-order generation. The RF tone is generated with an RF synthesizer (Holzworth HSM1800B) and then amplified (MiniCircuits TVA-82-213A+) to drive the modulator at high nonlinearity. An optical coupler is used to get the tap out of the MZM for null bias control. The bias control of IF MZM and the upconverter MZM is done using a custom bias controller unit built in-house. The optical signal is then amplified using an erbium-doped fiber amplifier (Pritel FA20) to improve the optical signal power so that 8 dBm power falls on the photodetector, which is required to have a sufficient link gain. A 100 GHz optical filter (ITU DWDM C30) is used to filter the out-of-band amplified spontaneous emission (ASE) noise. The optical signal is then passed through a 2 km fiber to emulate a BBU connected to a RRH at a different physical location. The out-of-band emissions at the output of the photodetector are filtered using a cavity filter (MiniCircuits ZVBP-25875-K+) and then passed to an RF amplifier to raise the power levels for appreciable EVM measurement from the signal analyzer. The output of the amplifier is then analyzed by a signal analyzer (Keysight N9040B UXA) to measure EVM performance and other critical performance metrics.

The experimental setup of a quadrupler closely follows as that of an optical doubler, with a change being the upconverter replaced with a DPMZM (iXblue MXIQ-LN-30)for quadrupler operation (Fig.6). The biasing of the DPMZM operating at quadrupling is performed without automatic bias control. The second-order generation at a null point is not as high as a first-order generation which is required for the doubler, with the same modulation depth. An erbium-doped fiber amplifier (EDFA) is used before the DPMZM stage to account for the additional losses in the DPMZM. The RF tone is applied to the RF ports of the child modulators via a 90 deg RF hybrid

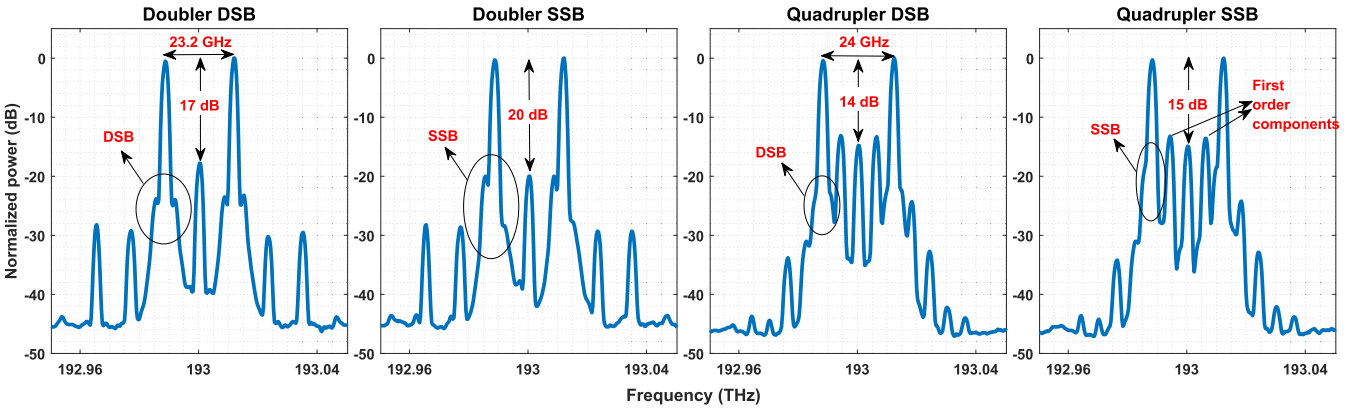

FIGURE 8. Optical spectrum of doubler with DSB format, SSB format, and quadrupler with DSB and SSB format (left to right). OSA resolution: 1.75 GHz.

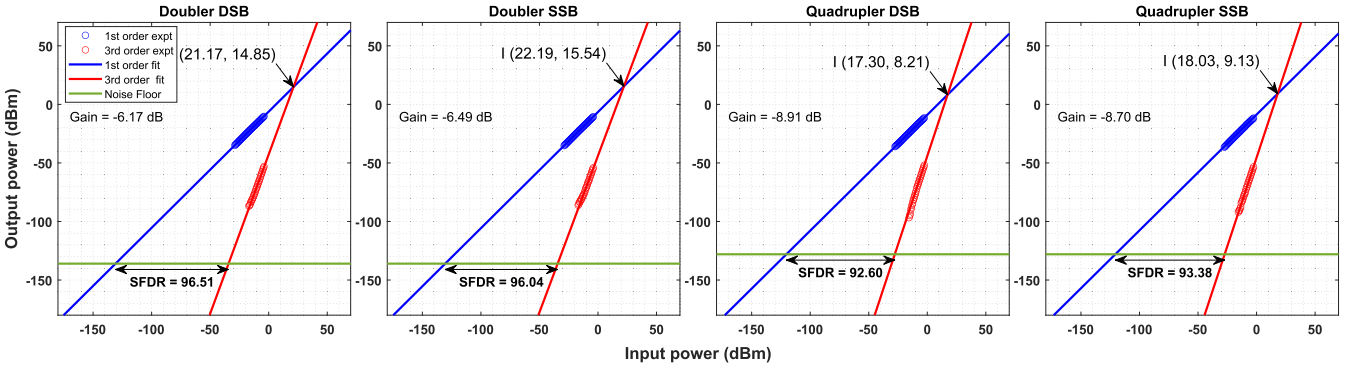

FIGURE 9. Third order intermodulation distortion(IMD3) performance of optical upconverting setups. SFDR - spurious free dynamic range; I - third order intercept.

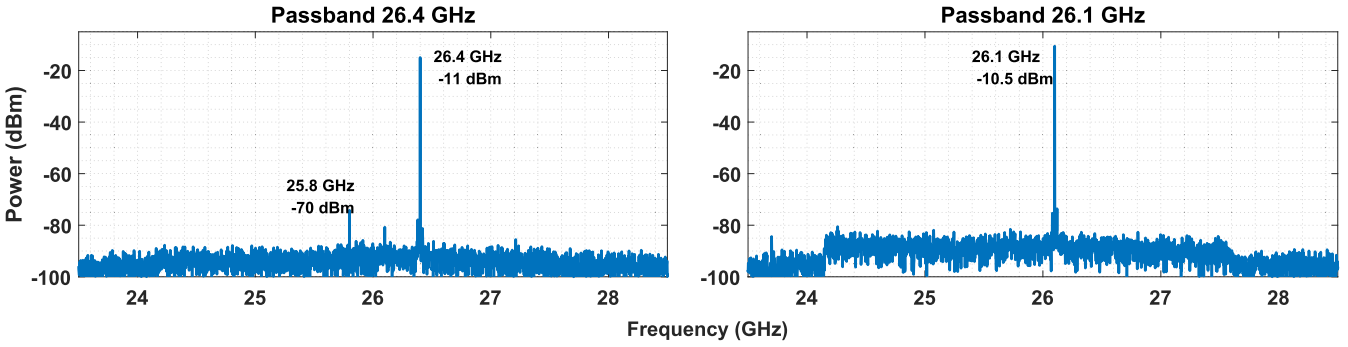

FIGURE 10. Sample spectrum of DSB optical doubler at 26.4 GHz (left) and quadrupler at 26.1 GHz (right) passband frequencies.

coupler through an RF amplifier and the modulation depth is only limited by the RF power rating of the DPMZM. The optical doubler and quadrupler experiments were conducted for both DSB and SSB formats.

For SSB modulation, the same IF MZM is used in the dual drive mode in the configuration shown in Fig.7. For experimental purposes, the same DDMZM is used for optical DSB modulation well, by terminating one of the input RF ports.

For experimental comparisons, electrical back-to-back (EB2B) and external modulation at 26.4 GHz are also performed in a standard RFoF configuration, shown in Fig.2. For both cases, the vector signal generator's (VSG) upconversion frequency is set to operate at 26 GHz. For the external modulation setup, the 26.4 GHz is directly fed to MZM, and no EDFA was employed after it, as the losses are far minimal without the doubler or quadruple stage. As there are no RF tone harmonics as compared to doubler or

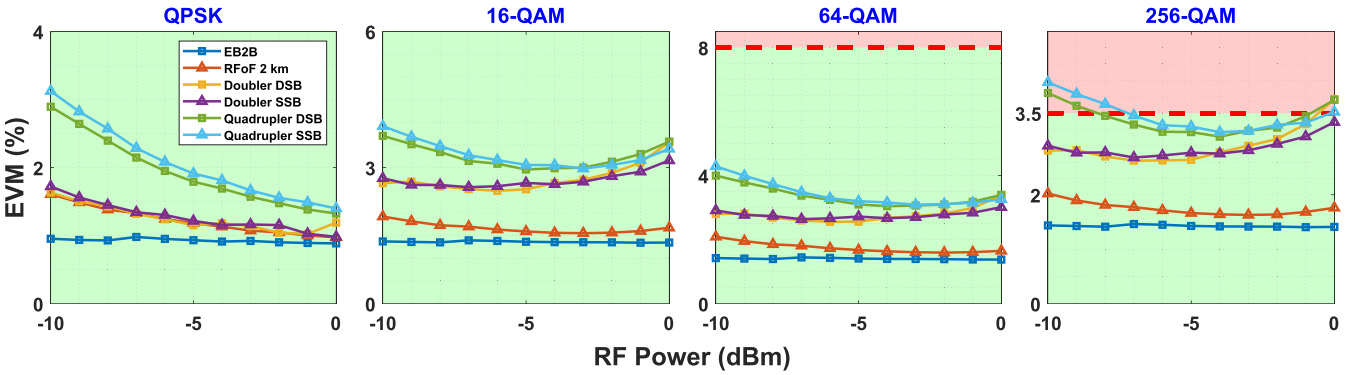

FIGURE 11. EVM performance of QPSK, 16-QAM, 64-QAM, and 256-QAM against the variation of input RF power to IF modulator. EVM limits are separated by dotted red lines in the plots. Note: the EVM limits of QPSK and 16-QAM are much higher than the plot range and are not shown. EB2B - Electrical back-to-back; RFoF - radio frequency over fiber.

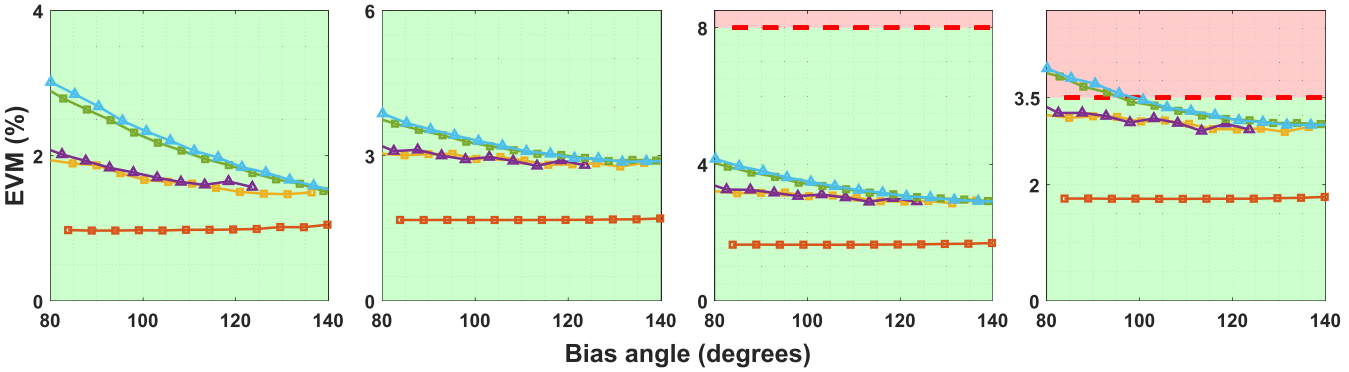

FIGURE 12. EVM performance of QPSK, 16-QAM, 64-QAM, and 256-QAM against the variation of bias angle. Figure legend and order of modulation follows the same as Fig.11.

quadrupler, this setup is used without the use of a cavity filter. For the rest of the paper, the external modulation scheme will be referred to as RFoF. For the EB2B case, an RF cable length of 6 ft (MiniCircuits E40-6FT-KMKM+) was used, and for the RFoF case, a standard single-mode fiber of length 2 km was used.

IV. RESULTS

A. OPTICAL SPECTRA

Fig.8 shows the optical spectra of all the discussed upconversion formats. The optical carrier suppression for the doubler configurations is observed as 17 dB and 20 dB for DSB and SSB, respectively. The optical carrier suppression for the quadrupler configurations is observed as 14 dB and 15 dB for DSB and SSB, respectively. For the quadrupler case, the first-order suppression is observed to be above 13 dB for both cases. It is to be noted that better suppression is achievable with better bias controllers but is sufficient for the scope of this experiment as the beat components generated due to its presence are already filtered out electrically using a cavity filter. The data sidebands in the case of optical quadrupler at 2.4 GHz are barely discernible in the plots due to the limited spectral resolution of the OSA (Finisar 100s - 1.75 GHz).

B. INTERMODULATION DISTORTION

For any analog system, one of the key performance matrices is the dynamic range of the system with measurement of third-order intermodulation distortion (IMD3). The IMD3 tests were carried out with a two-tone test to measure the spurious free dynamic range (SFDR) of the link established for each configuration [43]. Two tones seperated by 2 MHz were fed at 3.2 GHz nad 2.4 GHz, respectively, to the IF MZMs of doubler and quadrupler setups, and the measurements were done at 26.4 GHz (at the output RF amplifier). The noise floor of doubler and quadrupler were observed to be −136 dBm/Hz and −128 dBm/Hz, respectively. The noise degradation in quadrupler can be accounted to the two sets of EDFAs used, which is also briefed in section IV-C. Fig 9 shows the IMD3 plots of all upconverter setups, where the SFDR and third-order intercept (denoted as I) are shown. The experiments were carried out with 8 dBm optical input power falling on the photodetector in all the setups. The link gains (upconverted) observed are thus −6.16 dB, −6.48 dB, −8.90 dB, and −8.70 dB, respectively, for doubler DSB, doubler SSB, quadrupler DSB, and quadrupler SSB. The SFDR and thrid order intercept points of the individual setups are also shown in Fig.9

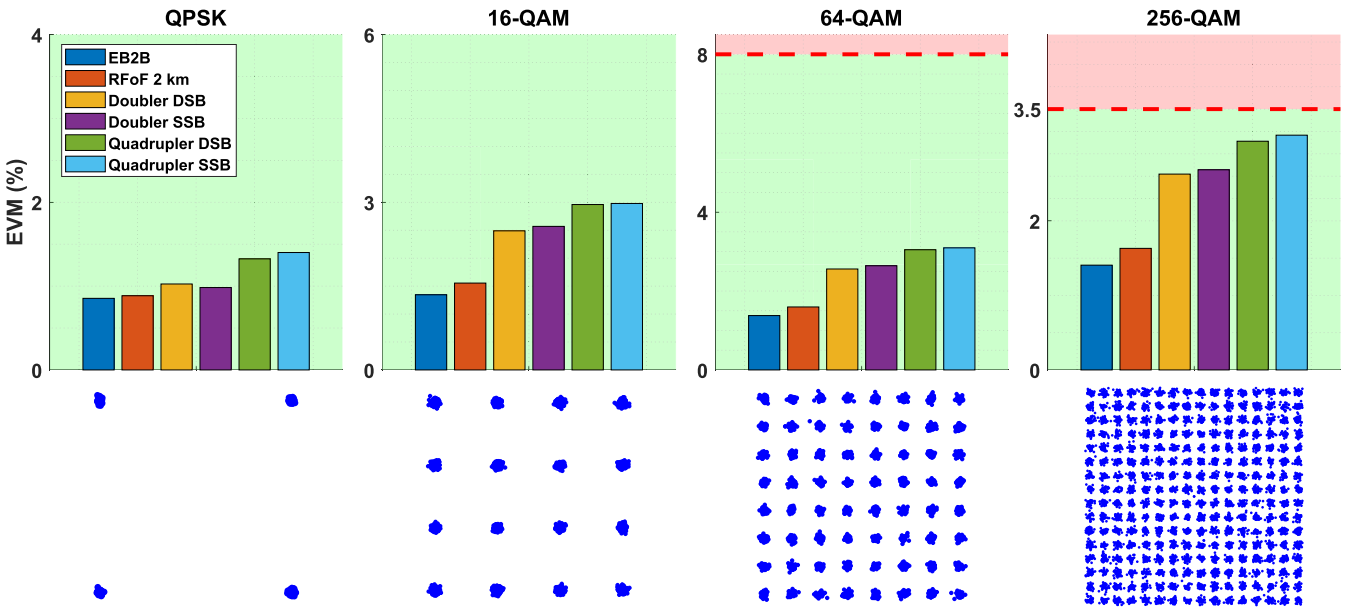

FIGURE 13. Best EVM performance of QPSK, 16 QAM, 64 QAM and 256 QAM for EB2B, ARoF, doubler and quadrupler setups at 26.4 GHz. The constellation of the worst-case EVM performance in each case, quadrupler SSB format is shown below each section. EVM limits are separated by dotted red lines in the plots. EB2B - Electrical back-to-back; ARoF - Analog radio over fiber.

C. OUT OF BAND EMISSIONS

The OBUE emission requirements are met with the appropriate choice of the RF cavity filter. As briefly mentioned in section II-C, the target harmonic tone suppression for the scope of this work is set at > 48 dB of data band power. Fig.10 (left) shows a sample spectrum of an SSB optical doubler with a passband at 26.4 GHz, which shows a qualified signal, with the nearest spurious suppressed by > 59 dB. It must be noted that the spectrum here is shown to a specific range of interest, and other bands outside the limits have higher suppression, even > 90 dB.

For the case of an optical quadrupler, 26.4 GHz was not the suitable candidate passband frequency for the available cavity filter. The $4f_{RF}$ and $4f_{RF} - f_{IF}$ appear at 24 GHz and 21.6 GHz, respectively, which are the highest spurious tones. While the aforementioned tones aren't fully suppressed, the EVM measurements were unaffected. With the available cavity filter, a candidate center frequency of 26.1 GHz complies with the emission requirements as shown in Fig. 10 (right).

D. EVM PERFORMANCE

The EVM performances were analyzed for all configurations for different modulation formats and are compared with the EB2B and RFoF formats (Fig.11 and Fig.12). For the EB2B case, the RF power was varied to find the optimal operating point while for the optical setups, the RF power and bias points were varied. At the lower RF powers, the EVM is limited by the noise while at the higher RF powers, it is degraded due to nonlinear components - the observation which is otherwise termed as 'EVM bathtub curve'. For EB2B, the third-order nonlinearity arises from the RF source, while for optical setups, the third-order nonlinearity is dominated by the transfer curve of the MZM [43]. For optical setups, low biasing (see Fig.2b), away from the quadrature point is found to be optimal. For the cases of optical doubler and quadrupler, the low biasing also provides smaller optical carrier power, which leads to weaker carrier components at PD output, which is an advantage as it relaxes the strict specifications of the RF filter [32], [33]. While further low biasing provides better EVM, one must note that the RF power of the passband signal also reduces correspondingly and thus will correspond to a requirement of further amplifier stages. For the parameter variations Fig.11, the bias point was fixed at 120 degrees - a point which was providing a better RF power (> -10 dBm after RF amplifier) and a relatively better EVM. For the parameter variations Fig.12, the input RF power (at IF modulator) was kept constant at -4 dBm - which was found to be the range of best operating points (mostly for the case of doubler and quadrupler).

Fig.13 shows the best EVM performance of all the tested formats. For all the plots, the EVM requirements as per 3GPP requirement are shaded red, and the acceptable levels are shaded green. From Fig.13, it can be observed that the EVM performance of EB2B and ARoF are better compared to the other optical upconversion formats. The extra penalty of ARoF compared to EB2B can be accounted for by the nonlinearity of the modulator. The optical upconversion formats deteriorate much further compared to the ARoF case - which is most likely due to the presence of optical amplifiers which reduces the SNR. While the optical doubler fares much better in all modulation formats than the optical quadrupler, both methods still fall below the required 3GPP 5G requirements. The performance of SSB modulation formats compares as fairly similar to that of the DSB format.

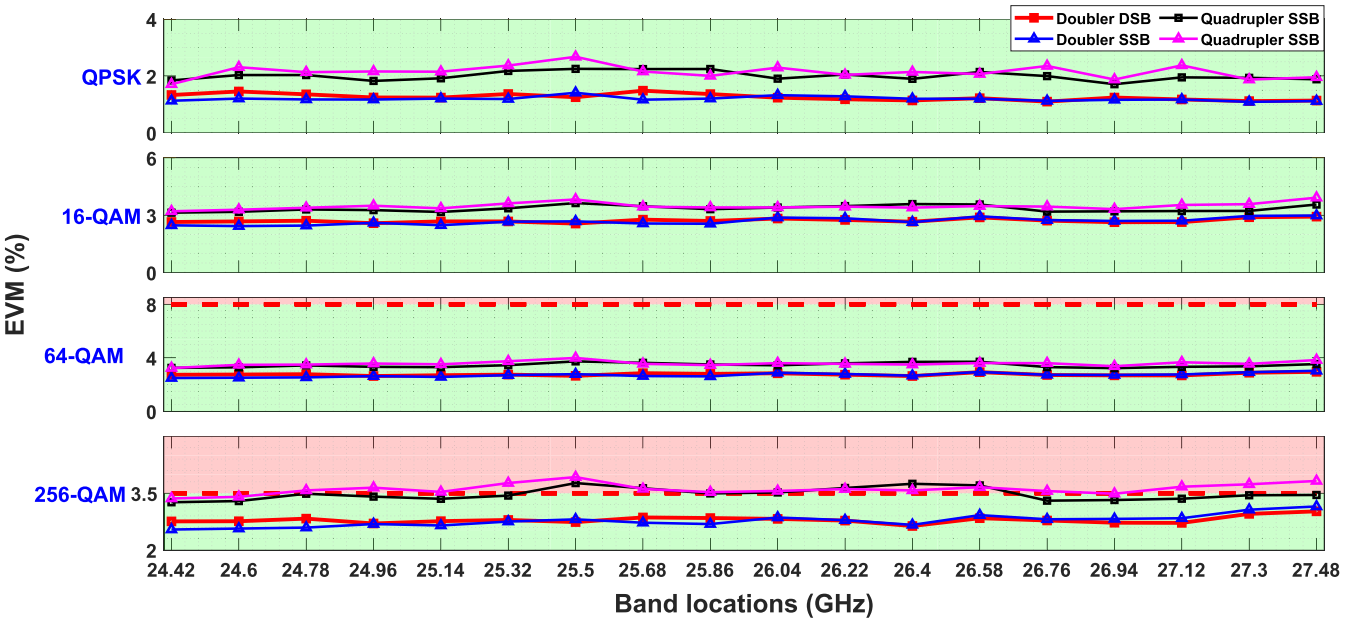

FIGURE 14. Tunability in the n258 band (24.25 - 27.5 GHz) for all modulation formats. EVM limits are separated by dashed red lines in the plots.

The advantage of the SSB modulation format is expected to be better only at longer transmission distances.

While the EVM requirement for 256 QAM is the lowest at 3.5%, the signal degradation affects this modulation format the most, which is evident from Fig. 13. Doubler has a higher margin to the limit than the case of quadrupler. At the measurement point (Fig. 5) for upconversion setups, while a mean active channel power less than -8 dBm is achieved, in practical scenarios, power amplifiers and beamforming components are used. At optimal operating conditions, achieving sufficient EVM at the point of wireless transmission is possible, with the margins achieved in this experiment. Up to 64 QAM have sufficient clearance to qualify for the 3GPP 5G standard, while 256 QAM is nearly at the limit.

E. TUNABILITY IN THE N258 BAND

For the doubler and quadrupler systems, the passband frequency can be adjusted by correspondingly tuning the RF tone. Fig.14 shows the EVM performance of the doubler and quadrupler setups, for both SSB and DSB formats; tuned across the n258 band (24.25 - 27.5 GHz). A set of eighteen equispaced frequencies are chosen here to demonstrate the tunability. In the case of the doubler setup, the IF tone was set at 3.2 GHz, and for the quadrupler setup, the IF tone was set at 2.4 GHz; where carrier frequency was continuously tuned. For the experiments demonstrating tuneability, the RF bandpass filter was removed due to the unavailability of corresponding filters for each spot frequency selected at the lab. The carrier frequency was continuously tuned, while the IF was fixed constant to achieve the tunability. The EVM performance is degraded compared to results shown in Fig.13 since the cavity filter is removed in these experiments. Even with the consequent out-of-band components, QPSK, 16-QAM, and 64-QAM are well within the limits.

F. DISCUSSIONS

Fig.13 shows that the EVM is slightly more degraded more for SSB compared to DSB even though SSB offers better resilience to dispersive fading. As shown in Fig.4, the overall power with SSB is lower and hence requires slightly higher optical amplification (or electrical amplification after photodetector), with a consequent slight degradation in SNR and hence in EVM. The benefits of SSB is expected to be evident in higher operating frequencies. While the multiband tests in the aforementioned experiments were limited by the availability of RF filters in our lab, EVM measurements show acceptable performance. This would mean that each frequency band requires its own filters for accurate EVM measurements. While cavity filters are bulky compared to surface mount components, they offer very low insertion loss and offer high rejection to out of band (OOB) components.

The use of optical amplifiers was necessary for achieving the link gain and providing sufficient SNR. The doubler setup uses a single EDFA, while the quadrupler uses two EDFAs in the path to compensate for the bias loss and the insertion loss of DPMZM. Thus, the ASE noise added in the quadrupler system is higher than the one in doubler. The EVM degradation of the quadrupler system can be accounted for this noise addition. Phase noise degradation can be another factor that affect the EVM performance of the quadrupler system, as compared to doubler. In general, a frequency multiplication system encounters a phase noise degradation of $20log_{10}(m)$, where m is the multiplication factor [44]. The

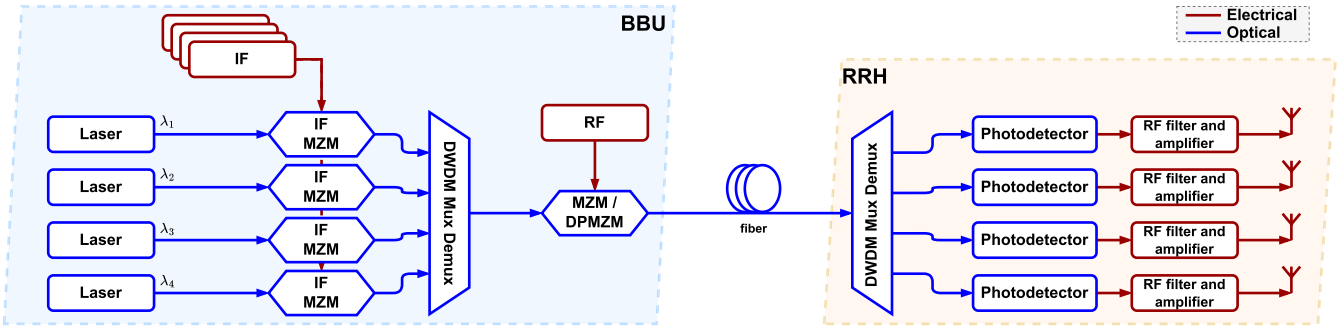

FIGURE 15. Multi-channel setup if optical upconversion schemes with a single upconverter stage for four channels.

above expression is valid only for the carrier component, and the upconverted component contains further degraded signal, which is a product of RF and IF components.

A major advantage of two-stage optical upconversion systems is the ease of performing optically multiplexing [45]. DWDM can be implemented to multiple IF data channels and can be combined to perform a single upconversion for all channels, as shown in Fig. 15. In the conceptual diagram given in Fig. 15, a case of transport from BBU to RRH, four DWDM channels along with four IF modulators are used to modulate the data bands and are then combined with DWDM mux/demux. The combined signal is then upconverted (doubled/quadrupled) with a single modulator. As the process is an electro-optic conversion, all the channels are modulated with the same modulation depth. The upconverted signal can then be transported to the RRH site, where DWDM demultiplexing is performed, and the signal is split into multiple antenna elements. In actual implementations, the electrical output is conditioned and given to phased array antennas for each channel. The added advantage of combined upconversion is that they can be used for advanced schemes such as coordinated multipoint (CoMP) [46], where multiple RRHs synchronously connect with a single user equipment.

As mentioned before, the scope of the experimental results in the paper deals with the downlink, and the uplink is not discussed. The major hurdle of the 'generation of mmWave' is non-existent in the uplink, as the signal is generated by the user equipment. The transport of the uplink can be done by a simple RFoF link - which is already demonstrated in the experimental results. With dispersion being the only issue at longer distances, a remote carrier delivery can also be done as shown in [20], where an unmodulated tone is transported with just upconversion so that IF conversion can be done at RRH for the uplink data. The scheme can also lower the requirement of high bandwidth modulator at the RRH.

Along with the size and complexity reduction of the RRH unit, power consumption can also be drastically improved with the proposed system or any other ARoF system as well. For a quick comparison, the RRH developed for the 5G Testbed project at IIT Madras, consumes a total of 192 W - with split of approximately 96 W each for FPGA/RFSOC and power amplifier with beamforming setup. [47] The RRH unit supports 4 channels of data streams with four beamforming antennas of 8 × 8 elements in each. For the setup discussed in Fig.5, the RRH elements are the photodetector and RF amplifier, which consume a total of 3W combined. For the uplink assumed as RFoF, considering a front-end amplifier and laser, the total power consumption is about 5 W. Hence, for a single-channel uplink and downlink, the total power consumption is around 8 W, and thus a four-channel system consumes 32 W power. Thus, a total of 128 W (optics:32 W + beamforming:96 W) is estimated for the ARoF system, which would amount to 33 % power savings.

Summarizing, the key contribution of this work is the first-time demonstration of upconversion schemes for 5G mmWave fronthauling for up to 256-QAM modulation. We have analyzed the critical signal quality parameters, such as EVM, SFDR, and out-of-band emissions, for different modulation formats and frequencies. We compare the performances of both doubling and quadrupling schemes and prove that, the performance degradation for quadrupler is minimal compared to the doubler; the data transported in both the schemes are within the EVM limit specified by 3GPP for up to 256-QAM modulation

V. CONCLUSION

In this paper, we have proposed and experimentally demonstrated optical fronthaul systems based on frequency doubling and quadrupling techniques, which can generate mmWave signals at the RRH thus reducing complexity. We also demonstrate an RFoF transmission and compare it with those of frequency multiplier schemes. We have experimentally demonstrated the generation and transmission of 26.4 GHz OFDM signals with modulation formats QPSK, 16 QAM, 64 QAM, and 256 QAM, and evaluated the systems' performances at the optimized operating point. The demonstrated upconversion systems are more resilient to dispersion-induced fading than conventional radio over fiber solutions. Moreover, upconversion schemes ensure that the modulators required at the front end are of lower bandwidth. We have also investigated the tunability and scalability of the systems across the n258 band and shown the feasibility of implementing dense wavelength division multiplexing

(DWDM) for multi sector antennas. The results show that the proposed systems can achieve EVM values meeting the 3GPP 5G standard requirements and therefore support high data rate transmission for future wireless networks.

REFERENCES

[1] J. G. Andrews, S. Buzzi, W. Choi, S. V. Hanly, A. Lozano, A. C. Soong, and J. C. Zhang, "What will 5G be?" *IEEE J. Sel. Areas Commun.*, vol. 32, no. 6, pp. 1065–1082, Jun. 2014.

[2] M. Shafi, A. F. Molisch, P. J. Smith, T. Haustein, P. Zhu, P. De Silva, F. Tufvesson, A. Benjebbour, and G. Wunder, "5G: A tutorial overview of standards, trials, challenges, deployment, and practice," *IEEE J. Sel. Areas Commun.*, vol. 35, no. 6, pp. 1201–1221, Jun. 2017.

[3] Y. Xiaohu et al., "Towards 6G wireless communication networks: Vision, enabling technologies, and new paradigm shifts," *Sci. China Inf. Sci.*, vol. 64, Jan. 2020, Art. no. 110301.

[4] S. Dang, O. Amin, B. Shihada, and M. S. Alouini, "What should 6G be?" *Nature Electron.*, vol. 3, pp. 20–29, Jan. 2020.

[5] W. Saad, M. Bennis, and M. Chen, "A vision of 6G wireless systems: Applications, trends, technologies, and open research problems," *IEEE Netw.*, vol. 34, no. 3, pp. 134–142, May 2020.

[6] *Spectrum for 6G Explained | Nokia*. Accessed: Jun. 27, 2023. [Online]. Available: https://www.nokia.com/about-us/newsroom/articles/spectrum-for-6G-explained/

[7] "IEEE 5G and beyond technology roadmap white paper," White Paper, 2017. [Online]. Available: https://futurenetworks.ieee.org/images/files/pdf/ieee-5g-roadmap-white-paper.pdf

[8] M. Matinmikko-Blue, "Sustainability and spectrum management in the 6G ERA," in *Proc. ITU Kaleidoscope, Connecting Phys. Virtual Worlds (ITU K)*, Geneva, Switzerland, 2021, pp. 1–9, doi: 10.23919/ITUK53220.2021.9662089.

[9] H. Viswanathan and P. E. Mogensen, "Communications in the 6G era," *IEEE Access*, vol. 8, pp. 57063–57074, 2020.

[10] Y. Niu, Y. Li, D. Jin, L. Su, and A. V. Vasilakos, "A survey of millimeter wave communications (mmWave) for 5G: Opportunities and challenges," *Wireless Netw.*, vol. 21, no. 8, pp. 2657–2676, 2015.

[11] T. S. Rappaport, S. Sun, R. Mayzus, H. Zhao, Y. Azar, K. Wang, G. N. Wong, J. K. Schulz, M. Samimi, and F. Gutierrez, "Millimeter wave mobile communications for 5G cellular: It will work!" *IEEE Access*, vol. 1, pp. 335–349, 2013.

[12] I. Chih-Lin, H. Li, J. Korhonen, J. Huang, and L. Han, "RAN revolution with NGFI (xhaul) for 5G," *J. Lightw. Technol.*, vol. 36, no. 2, pp. 541–550, Jan. 15, 2018.

[13] T. Pfeiffer, "Next generation mobile fronthaul and midhaul architectures [Invited]," *J. Opt. Commun. Netw.*, vol. 7, no. 11, pp. B38–B45, Nov. 2015.

[14] I. Chih-Lin, Y. Yuan, J. Huang, S. Ma, C. Cui, and R. Duan, "Rethink fronthaul for soft RAN," *IEEE Commun. Mag.*, vol. 53, no. 9, pp. 82–88, Sep. 2015.

[15] C. Ranaweera, E. Wong, A. Nirmalathas, C. Jayasundara, and C. Lim, "5G C-RAN with optical fronthaul: An analysis from a deployment perspective," *J. Lightw. Technol.*, vol. 36, no. 11, pp. 2059–2068, Jun. 2018.

[16] C. Lim and A. Nirmalathas, "Radio-over-fiber technology: Present and future," *J. Lightw. Technol.*, vol. 39, no. 4, pp. 881–888, Feb. 2021.

[17] T. R. Raddo, S. Rommel, I. T. Monroy, C. Vagionas, G. Kalfas, and N. Pleros, "Analog radio-over-fiber 5G fronthaul systems: BlueSPACE and 5G-PHOS projects convergence," in *Proc. Eur. Conf. Netw. Commun. (EuCNC)*, Jun. 2019, pp. 479–484.

[18] Y. Tian, K. L. Lee, C. Lim, and A. Nirmalathas, "60 GHz analog radio-over-fiber fronthaul investigations," in *Proc. Opt. Fiber Commun. Conf. Expo. (OFC)*, vol. 1, 2017, pp. 4304–4310.

[19] L. Bogaert, J. Van Kerrebrouck, H. Li, I. L. De Paula, K. Van Gasse, C. Y. Wu, P. Ossieur, S. Lemey, H. Rogier, P. Demeester, G. Roelkens, J. Bauwelinck, and G. Torfs, "SiPhotonics/GaAs 28-GHz transceiver with reflective EAM for laser-less mmWave-over-fiber," *J. Lightw. Technol.*, vol. 39, no. 3, pp. 779–786, Feb. 1, 2021.

[20] S. Rommel, E. Grivas, B. Cimoli, D. Dodane, A. Morales, E. Pikasis, J. Bourderionnet, G. Feugnet, J. Barros Carvalho, M. Katsikis, K. Ntontin, D. Kritharidis, I. Spaleniak, P. Mitchell, M. Dubov, and I. Tafur Monroy, "Real-time high-bandwidth mm-wave 5G NR signal transmission with analog radio-over-fiber fronthaul over multi-core fiber," *EURASIP J. Wireless Commun. Netw.*, vol. 2021, no. 1, p. 43, 2021.

[21] A. Tsakyridis, E. Ruggeri, G. Kalfas, R. M. Oldenbeuving, P. W. Van Dijk, C. G. Roeloffzen, Y. Leiba, A. Miliou, N. Pleros, and C. Vagionas, "Reconfigurable fiber wireless IFoF fronthaul with 60 GHz phased array antenna and silicon photonic ROADM for 5G mmWave C-RANs," *IEEE J. Sel. Areas Commun.*, vol. 39, no. 9, pp. 2816–2826, Sep. 2021.

[22] L. Maleki, "Recent progress in opto-electronic oscillator," in *Proc. Int. Top. Meeting Microw. Photon.*, vol. 53, Oct. 2005, pp. 81–84.

[23] J. Yao, "Microwave photonics," *J. Lightw. Technol.*, vol. 27, no. 3, pp. 314–335, Feb. 1, 2009.

[24] L. Goldberg, H. Taylor, J. Weller, and D. Bloom, "Microwave signal generation with injection-locked laser diodes," *Electron. Lett.*, vol. 19, no. 13, p. 491, 1983.

[25] Z. F. Fan, "Optical generation of a megahertz-linewidth microwave signal using semiconductor lasers and a discriminator-aided phase-locked loop," *IEEE Trans. Microw. Theory Techn.*, vol. 45, no. 8, pp. 1296–1300, Aug. 1997.

[26] J. O'Reilly, P. Lane, R. Heidemann, and R. Hofstetter, "Optical generation of very narrow linewidth millimetre wave signals," *Electron. Lett.*, vol. 25, no. 28, pp. 2309–2311, 1992.

[27] R. Maldonado-Basilio, M. Hasan, R. Guemri, F. Lucarz, and T. J. Hall, "Generalized Mach–Zehnder interferometer architectures for radio frequency translation and multiplication: Suppression of unwanted harmonics by design," *Opt. Commun.*, vol. 354, pp. 122–127, Nov. 2015.

[28] J. Zhang, H. Chen, M. Chen, T. Wang, and S. Xie, "A photonic microwave frequency quadrupler using two cascaded intensity modulators with repetitious optical carrier suppression," *IEEE Photon. Technol. Lett.*, vol. 19, no. 14, pp. 1057–1059, Jul. 2007.

[29] H. Chi and J. Yao, "Frequency quadrupling and upconversion in a radio over fiber link," *J. Lightw. Technol.*, vol. 26, no. 15, pp. 2706–2711, Aug. 2008.

[30] S. Yu, W. Gu, A. Yang, T. Jiang, and C. Wang, "A frequency quadrupling optical mm-wave generation for hybrid fiber-wireless systems," *IEEE J. Sel. Areas Commun.*, vol. 31, no. 12, pp. 797–803, Dec. 2013.

[31] M. Mohamed, X. Zhang, B. Hraimel, and K. Wu, "Analysis of frequency quadrupling using a single Mach–Zehnder modulator for millimeter-wave generation and distribution over fiber systems," *Opt. Exp.*, vol. 16, no. 14, pp. 10786–10802, 2008.

[32] S. J. Sreeraj, B. Lakshman, R. Ganti, D. Koilpillai, and D. Venkitesh, "Frequency doubler based optical generation and transport of 5G mmWave signals for fronthauling," in *Proc. Opt. InfoBase Conf. Papers*, pp. 5–6, 2022.

[33] S. J. Sreeraj, D. Venkitesh, R. D. Koilpillai, and A. Nirmalathas, "Analog optical generation and transport for 5G millimeter wave systems," in *Proc. IEEE Photon. Conf. (IPC)*, Oct. 2021, pp. 1–2.

[34] S. Rommel, D. Perez-Galacho, J. M. Fabrega, R. Muñoz, S. Sales, and I. Tafur Monroy, "High-capacity 5G fronthaul networks based on optical space division multiplexing," *IEEE Trans. Broadcast.*, vol. 65, no. 2, pp. 434–443, Jun. 2019.

[35] C. T. Lin, P. T. Shih, J. Chen, W. Q. Xue, P. C. Peng, and S. Chi, "Optical millimeter-wave signal generation using frequency quadrupling technique and no optical filtering," *IEEE Photon. Technol. Lett.*, vol. 20, no. 12, pp. 1027–1029, Jun. 2008.

[36] F. Zhang, Q. Guo, and S. Pan, "Photonics-based real-time ultra-high-range-resolution radar with broadband signal generation and processing," *Sci. Rep.*, vol. 7, no. 1, pp. 1–8, Oct. 2017.

[37] G. H. Smith, D. Novak, and Z. Ahmed, "Technique for optical SSB generation to overcome dispersion penalties in fibre-radio systems," *Electron. Lett.*, vol. 33, no. 1, pp. 74–75, 1997.

[38] C. H. Lee, *Microwave Photonics*, vol. 24. Boca Raton, FL, USA: CRC Press, 2007.

[39] G. H. Smith, D. Novak, and Z. Ahmed, "Overcoming chromatic-dispersion effects in fiber-wireless systems incorporating external modulators," *IEEE Trans. Microw. Theory Techn.*, vol. 45, no. 8, pp. 1410–1415, Aug. 1997.

[40] T. S. Rappaport, Y. Xing, O. Kanhere, S. Ju, A. Madanayake, S. Mandal, A. Alkhateeb, and G. C. Trichopoulos, "Wireless communications and applications above 100 GHz: Opportunities and challenges for 6G and beyond," *IEEE Access*, vol. 7, pp. 78729–78757, 2019.

[41] C. T. Lin, J. Chen, S. P. Dai, P. C. Peng, and S. Chi, "Impact of nonlinear transfer function and imperfect splitting ratio of MZM on optical up-conversion employing double sideband with carrier suppression modulation," *J. Lightw. Technol.*, vol. 26, no. 15, pp. 2449–2459, Aug. 2008.

[42] 3GPP, *Base Station (BS) Radio Transmission and Reception*, document ETSI TS 138 104, Release 16, 3rd Generation Partnership Project (3GPP), 2023.
[43] D. Marpaung, "High dynamic range analog photonic links: Design and implementation," Ph.D. thesis, Univ. Twente, Enschede, The Netherlands, 2009, doi: https://doi.org/10.3990/1.9789036528603.
[44] A. Kanno and T. Kawanishi, "Millimeter-wave signal generation using cascaded optical frequency multiplication technique," in *Proc. 44th Eur. Microw. Conf.*, Oct. 2014, pp. 1028–1031.
[45] P.-T. Shih, C.-T. Lin, W.-J. Jiang, J. J. Chen, H.-S. Huang, Y.-H. Chen, P.-C. Peng, and S. Chi, "WDM up-conversion employing frequency quadrupling in optical modulator," *Opt. Exp.*, vol. 17, no. 3, pp. 1726–1733, 2009.
[46] Y. Tian, K.-L. Lee, C. Lim, and A. Nirmalathas, "Performance evaluation of CoMP for downlink 60-GHz radio-over-fiber fronthaul," in *Proc. Int. Topical Meeting Microw. Photon. (MWP)*, Oct. 2017, pp. 1–4.
[47] *5G Testbed IIT Madras*. Accessed: Oct. 11, 2023. [Online]. Available: http://www.5gtbiitm.in/index.php/home/

S. J. SREERAJ (Graduate Student Member, IEEE) received the B.Tech. degree in electronics and communication engineering from the University of Kerala, India, in 2014, and the M.Tech. degree in communication engineering and signal processing from Amrita Viwsa Vidyapeetham, Coimbatore, India, in 2017. He is currently pursuing the Ph.D. degree in electrical engineering with the Indian Institute of Technology Madras, Chennai, India. His research interests include analog radio over fiber systems for wireless systems, photonic radars, and optical communications.

B. LAKSHMAN (Graduate Student Member, IEEE) received the B.Tech. degree in electrical and electronics engineering from the SRM Institute of Science and Technology, India, in 2018. He is currently pursuing the M.S. degree in electrical engineering with the Indian Institute of Technology Madras, Chennai, India. His research interests include analog/RF/microwave and millimetre wave circuits and systems for 5G communications.

RADHAKRISHNA GANTI (Member, IEEE) received the B.Tech. and M.Tech. degrees in electrical engineering from the Indian Institute of Technology (IIT) Madras, Chennai, India, and the master's degree in applied mathematics and the Ph.D. degree in electrical engineering from the University of Notre Dame, in 2009. He is currently an Associate Professor with IIT Madras. He is the coauthor of the monograph, *Interference in Large Wireless Networks* (NOW Publishers, 2008). His doctoral work focused on the spatial analysis of interference networks using tools from stochastic geometry. He received the 2014 IEEE Stephen O. Rice Prize, the 2014 IEEE Leonard G. Abraham Prize, and the 2015 IEEE Communications Society Young Author Best Paper Award. He was also awarded the 2016–2017 Institute Research and Development Award (IRDA) by IIT Madras. In 2019, he was awarded the TSDSI Fellow for Technical Excellence in standardization activities and contribution to LMLC use case in ITU. He was the Lead PI from IITM involved in the development of 5G base stations for the 5G Testbed Project funded by the Department of Telecommunications, Government of India.

AMPALAVANAPILLAI NIRMALATHAS (Senior Member, IEEE) received the Ph.D. degree in electrical and electronic engineering from The University of Melbourne. He is currently a Professor and the Deputy Dean (Research) of the Faculty of Engineering and Information Technology. His current research interests include energy efficient telecommunications, access networks, optical-wireless network integration, mobile-access edge computing, photonic reservoir computing, the Internet of Things, and broadband wireless systems and devices. He has been the Chair of IEEE Photonics Society's Future Technologies Task Force, since 2021. He was also the Co-Chair of IEEE Future Networks Initiative's Optics Working Group, from 2020 to 2021. He is also the Deputy Co-Chair of National Committee on Information and Communication Sciences of the Australia. Academy of Sciences.

R. DAVID KOILPILLAI (Member, IEEE) received the B.Tech. degree in electrical engineering from the Indian Institute of Technology (IIT) Madras, and the M.S. and Ph.D. degrees in electrical engineering from the California Institute of Technology, Pasadena, CA, USA. In 2002, he joined the Electrical Engineering (EE) Faculty, IIT Madras. He is currently the Qualcomm Institute Chair Professor in EE and the Dean (Planning). From 2008 to 2009, he served as the Co-Chair of the IITM Special Task Force for setting up the new IIT Hyderabad. He was also the Head of the Central Electronics Centre, IIT Madras, from 2010 to 2011. His technical areas of expertise include cellular and broadband wireless systems, and DSP techniques for wireless communications. He is the Faculty Coordinator of the IITMSAT Student Satellite Initiative. In 2007, he was on sabbatical from IITM and he served as the Chief Scientist of the Centre of Excellence in Wireless Technology (CEWiT), a public–private research and development initiative of the Government of India, and he was responsible for launching the national project Broadband Wireless Consortium of India. Prior to joining IITM, he was with General Electric (GE) Corporate Research and Development for four years and Ericsson, USA, for eight years, where he held different technical and managerial positions. In 2000, he became the Director of the Ericsson's Advanced Technologies and Research Department, RTP, NC, USA, developing GPRS/EDGE handset technology. His technical contributions at GE and Ericsson have resulted in 32 U.S. patents, ten Canadian patents, and 19 WIPO/European patents. His current technical activities are in the areas of cellular evolution—4G and 5G, smart grid communications, and DSP for high speed coherent optical communications. He received the Ericsson Inventor of the Year Award, the highest technical recognition within Ericsson, in 1999. In 2003, he was an Elected Fellow of the Indian National Academy of Engineering. In 2014, he received the Srimathi Marti Annapurna Gurunath Award for Excellence in Teaching (Best Teacher Award of IIT Madras).

DEEPA VENKITESH (Member, IEEE) received the Ph.D. degree in physics from the Indian Institute of Technology (IIT) Bombay, Mumbai, India, in 2009. She is currently a Professor with the Department of Electrical Engineering, IIT Madras, Chennai, India. She has authored more than 100 publications in international peer-reviewed journals and conferences. Her research interests include optical communication systems, optical signal processing, and microwave photonics.